Transparent lateral boundary conditions for systems of equations which support barotropic, baroclinic, and potential vorticity waves.

A McDonald

Corresponding author address:
Aidan McDonald, Met Éireann, Glasnevin Hill, Dublin 9, Ireland.
E-mail: aidan.mcdonald@met.ie

(Manuscript received 12 May 2005, in final form 25 October 2005.)

ABSTRACT

Transparent boundary conditions are derived for three systems of linear equations which support potential vorticity waves as well as barotropic and baroclinic waves. The first system, the one-dimensional shallow water equations, supports potential vorticity and barotropic waves only and it is used to lay the foundations for the second, two-layer system, which supports baroclinic waves also, and for the third system, the two dimensional linearized hydrostatic primitive equations, which supports multiple baroclinic and potential vorticity waves. For each system of equations the derived boundary conditions are shown to be stable and accurate for practical integrations despite the presence of dispersive waves.

1. Introduction

In McDonald (2005), hereinafter called M05, transparent lateral boundary conditions were derived for two systems of linear equations which support baroclinic waves as well as barotropic waves. The purpose of this paper is to extend that work to systems of linear equations which also support potential vorticity waves by adding the Coriolis terms to the equations. The presence of these terms causes the waves to become dispersive and consequently the pivotal inverse transform becomes intractable. Fortunately, Engquist and Majda (1977) furnished a method for overcoming this difficulty. Their method gives rise to an increasingly accurate hierarchy of 'semi- transparent' boundary conditions, as is described in section 2 for the one dimensional shallow water model. In section 3 baroclinic waves are introduced via the simplest possible system of equations which supports barotropic, baroclinic, and potential vorticity waves: the two-layer model. In section 4 it is shown that semi-transparent boundary conditions can be derived for a linearized multi-level model by transforming the equations into a set of shallow water equations each with its own effective depth. Using the methods described in section 2 the boundary fields can be derived for each of these shallow water equations. Transforming these fields back to physical space completes the task of deriving semi-transparent boundary fields. These are then tested in a series of integrations and are shown to be stable and accurate.

2. A single layer model

The complication caused by the introduction of the Coriolis terms is that the waves become dispersive. The purpose of this section is to examine the implications of this for the construction of transparent (in fact, now semi-transparent, as we shall see) boundary conditions. To do so, the simplest possible system which supports both gravity and potential vorticity waves is chosen; the one-dimensional shallow water equations. Baroclinic waves are excluded in order to facilitate a derivation with a minimum of algebraic clutter. Thus, when they are introduced in the next section, and the complicated algebra proliferates, this section will serve as a template. More importantly, the boundary conditions for the multi-level model are derived in section 4 by projecting the equations of motion into a series of shallow water equations each with a different gravity-inertia wave velocity.

Therefore the boundary conditions derived in this section will also be used in section 4 for the multi-level model with a trivial re-definition of the gravity wave speed.

The equations are

$$\frac{\partial \eta}{\partial t} + \bar{u}\frac{\partial \eta}{\partial x} + H\frac{\partial u}{\partial x} = 0, \tag{2.1}$$

$$\frac{\partial u}{\partial t} + \bar{u}\frac{\partial u}{\partial x} + g\frac{\partial \eta}{\partial x} - fv = 0, \tag{2.2}$$

$$\frac{\partial v}{\partial t} + \bar{u}\frac{\partial v}{\partial x} + fu = 0, \tag{2.3}$$

where x and t are the space and time co-ordinates, and $g = 9.81$ is the gravitational acceleration, $\bar{u}$ is a constant advecting velocity, and $f = 10^{-4}$ is a constant Coriolis parameter. The field $\eta(x,t)$ describes the displacement of the fluid surface from its resting thickness, H. Lastly, $u(x,t)$ and $v(x,t)$ are the eastward and northward horizontal velocity components.

2.1 Derivation of the boundary conditions

Let $\mathbf{\Psi}$ be the vector (superscript 'T' denotes transpose)

$$\mathbf{\Psi} = (\eta, u, v)^T. \tag{2.4}$$

Taking the Laplace transform,

$$\hat{\mathbf{\Psi}}(x,s) = \int_0^\infty e^{-st}\mathbf{\Psi}(x,t)dt, \tag{2.5}$$

of eqs. (2.1) - (2.3) and using property 15 on page 210 of Doetsch (1971) yields

$$s\hat{\eta}(x,s) + \bar{u}\frac{\partial \hat{\eta}(x,s)}{\partial x} + H\frac{\partial \hat{u}(x,s)}{\partial x} = \eta(x,0_+), \tag{2.6}$$

$$s\hat{u}(x,s) + \bar{u}\frac{\partial \hat{u}(x,s)}{\partial x} + g\frac{\partial \hat{\eta}(x,s)}{\partial x} - f\hat{v}(x,s) = u(x,0_+), \tag{2.7}$$

$$s\hat{v}(x,s) + \bar{u}\frac{\partial \hat{v}(x,s)}{\partial x} + f\hat{u}(x,s) = v(x,0_+), \tag{2.8}$$

or, in matrix form,

$$\begin{bmatrix} \bar{u} & H & 0 \\ g & \bar{u} & 0 \\ 0 & 0 & \bar{u} \end{bmatrix} \frac{\partial}{\partial x} \begin{bmatrix} \hat{\eta} \\ \hat{u} \\ \hat{v} \end{bmatrix} (x,s) + s \begin{bmatrix} 1 & 0 & 0 \\ 0 & 1 & -f/s \\ 0 & f/s & 1 \end{bmatrix} \begin{bmatrix} \hat{\eta} \\ \hat{u} \\ \hat{v} \end{bmatrix} (x,s) = \begin{bmatrix} \eta \\ u \\ v \end{bmatrix} (x,0_+), \tag{2.9}$$

or, symbolically,

$$\mathbf{A}\frac{\partial\hat{\mathbf{\Psi}}(x,s)}{\partial x}+s\mathbf{B}\hat{\mathbf{\Psi}}(x,s)=\mathbf{\Psi}(x,0_+). \tag{2.10}$$

Comparing eqs. (2.10) and (2.9) makes the definitions of $\mathbf{A}$ and $\mathbf{B}$ obvious. Multiplying across by $\mathbf{A}^{-1}$ yields

$$\frac{\partial\hat{\mathbf{\Psi}}(x,s)}{\partial x}+s\mathbf{A}^{-1}\mathbf{B}\hat{\mathbf{\Psi}}(x,s)=\mathbf{A}^{-1}\mathbf{\Psi}(x,0_+), \tag{2.11}$$

where

$$\mathbf{A}^{-1}=\frac{1}{\bar{u}(\bar{u}^2-gH)}\begin{bmatrix}\bar{u}^2 & -\bar{u}H & 0\\ -\bar{u}g & \bar{u}^2 & 0\\ 0 & 0 & \bar{u}^2-gH\end{bmatrix}, \tag{2.12}$$

and

$$\mathbf{A}^{-1}\mathbf{B}=\frac{1}{\bar{u}(\bar{u}^2-gH)}\begin{bmatrix}\bar{u}^2 & -\bar{u}H & \bar{u}Hf/s\\ -\bar{u}g & \bar{u}^2 & -\bar{u}^2f/s\\ 0 & (\bar{u}^2-gH)f/s & (\bar{u}^2-gH)\end{bmatrix}. \tag{2.13}$$

If a matrix $\mathbf{Q}$ can be found such that

$$\mathbf{Q}^{-1}\mathbf{A}^{-1}\mathbf{B}\mathbf{Q}=\mathbf{\Lambda}, \tag{2.14}$$

where $\mathbf{\Lambda}$ is a diagonal matrix, then its diagonal elements consist of the eigenvalues of $\mathbf{A}^{-1}\mathbf{B}$, and $\mathbf{Q}^{-1}$ consists of its left eigenvectors. Defining Y to be

$$Y=\left\{1+\frac{f^2}{s^2}\left(1-\frac{\bar{u}^2}{\bar{c}^2}\right)\right\}^{\frac{1}{2}}, \tag{2.15}$$

where $\bar{c}=\sqrt{gH}$, the three eigenvalues are

$$\lambda_\pm=\frac{1}{\bar{u}\pm\bar{c}}\pm\frac{\bar{c}(1-Y)}{\bar{u}^2-\bar{c}^2};\qquad \lambda_{pv}=\frac{1}{\bar{u}}, \tag{2.16}$$

corresponding to the two gravity-inertia waves and the potential vorticity wave respectively. The left eigenvectors associated with these eigenvalues are, respectively

$$\mathbf{l}_\pm=n_\pm(s)\left(g,\ \pm\bar{c}Y,\ \frac{f}{s}\bar{u}\right);\qquad \mathbf{l}_{pv}=n_{pv}(s)\left(\frac{\bar{u}}{H}\frac{f}{s},\ \frac{f}{s},\ 1\right), \tag{2.17}$$

where $n_\pm(s)$ and $n_{pv}(s)$ are arbitrary normalization factors. Multiplying eq. (2.11) by $\mathbf{l}_k$ yields an equation, $(\mathbf{l}_1=\mathbf{l}_+,\mathbf{l}_2=\mathbf{l}_{pv},\mathbf{l}_3=\mathbf{l}_-)$,

$$\frac{\partial\mathbf{l}_k.\hat{\mathbf{\Psi}}(x,s)}{\partial x}+s\lambda_k\mathbf{l}_k.\hat{\mathbf{\Psi}}(x,s)=\mathbf{l}_k.\mathbf{A}^{-1}\mathbf{\Psi}(x,0_+), \tag{2.18}$$

whose solution is, see page 21 of Ince (1956),

$$\mathbf{l}_k.\hat{\mathbf{\Psi}}(x,s) = \mathbf{l}_k.\hat{\mathbf{\Psi}}(x_0,s)e^{-s\lambda_k(x-x_0)} + e^{-s\lambda_k x}\int_{x_0}^{x} \mathbf{l}_k.\mathbf{A}^{-1}\mathbf{\Psi}(\xi,0_+)e^{s\lambda_k\xi}d\xi. \tag{2.19}$$

Consider the λ_+-wave. If the arbitrary normalization factor, $n_+(s)$, is chosen to be 1, and it is assumed that terms of order f/s or higher make only a small contribution to the inverse Laplace transform of eq. (2.19) the result is, see property 9 on page 209 of Doetsch (1971),

$$[g\eta + \bar{c}u](x,t) = [g\eta + \bar{c}u]\left(x_0, t - \frac{x - x_0}{\bar{u} + \bar{c}}\right) + In_+^0. \tag{2.20}$$

If, on the other hand, $n_+(s) = s$ and it is assumed that terms of order $(f/s)^2$ or higher make only a small contribution to the inverse Laplace transform of eq. (2.19) the result is

$$\left[\frac{\partial(g\eta + \bar{c}u)}{\partial t} + f\bar{u}v\right](x,t) = \left[\frac{\partial(g\eta + \bar{c}u)}{\partial t} + f\bar{u}v\right]\left(x_0, t - \frac{x - x_0}{\bar{u} + \bar{c}}\right) + In_+^1. \tag{2.21}$$

Here In_+^k represents the contribution to the solution from the initial state, which is not of interest as far as deriving boundary conditions is concerned. In principle, this procedure can be continued, deriving solutions containing higher and higher time derivatives.

Consider a region of integration defined by $0 \leq x \leq L$, and $\bar{u} + \bar{c} > 0$, then what eq. (2.21) says is that if, at any time t the combination of fields on the right hand side is non-zero at $x_0 = 0$, then $x/(\bar{u} + \bar{c})$ seconds later this non-zero value will have been transported to the position x in the interior at a speed $(\bar{u} + \bar{c})$ ms^{-1}. Thus, to prevent this gravity-inertia wave from entering the region it is essential to maintain the condition $[\partial(g\eta + \bar{c}u)/\partial t + f\bar{u}v](0,t) = 0$ throughout the integration . By the same token, in a nested integration, if boundary fields are being supplied from an external 'host' model, designated by the superscript h, and they are such that $[\partial(g\eta^h + \bar{c}u^h)/\partial t + f\bar{u}v^h](0,t) \neq 0$ then this gravity-inertia wave will enter the integration area. If $\bar{u} + \bar{c} < 0$ the reasoning is the same except that it applies to the boundary at $x = L$.

If $n_{pv}(s) = 1$ and it is assumed that terms of order f/s or higher make only a small contribution to the inverse Laplace transform of eq. (2.19) the result is

$$v(x,t) = v\left(x_0, t - \frac{x - x_0}{\bar{u}}\right) + In_{pv}^0. \tag{2.22}$$

If $n_{pv}(s) = s$ then, to all orders of f/s,

$$\left[\frac{\partial v}{\partial t} + f\left(u + \frac{\bar{u}}{H}\eta\right)\right](x,t) = \left[\frac{\partial v}{\partial t} + f\left(u + \frac{\bar{u}}{H}\eta\right)\right]\left(x_0, t - \frac{x - x_0}{\bar{u}}\right) + In^1_{pv}. \tag{2.23}$$

Substituting u from eq.(2.3) yields

$$-\frac{1}{\bar{u}}\left[\frac{\partial v}{\partial t} + f\left(u + \frac{\bar{u}}{H}\eta\right)\right] = \frac{\partial v}{\partial x} - \frac{f\eta}{H}, \tag{2.24}$$

the potential vorticity for the system of equations (2.1)-(2.3). That it is conserved following the parcel can be seen by taking $\partial/\partial x$ of eq. (2.3) and subtracting f/H times eq. (2.1).

Now, repeating the above arguments, if $\bar{u} > 0$, in a nested integration, in order to inject potential vorticity into the integration at $x = 0$ via a host model, put $v(t,0) = v^h(t,0)$ to lowest order. To all higher orders put $[\partial v/\partial t + f(u + \bar{u}\eta/H)](0,t)$ equal to its host model value. If $\bar{u} < 0$ the reasoning is the same except that it applies to the boundary at $x = L$.

2.2 Time discretization of the boundary conditions

In this section is described how to derive an order-consistent set of discretized boundary conditions. First, some definitions. Write

$$\hat{W}_k = (\mathbf{Q^{-1}}\hat{\mathbf{\Psi}})_k \tag{2.25}$$

such that $\hat{W}_1, \hat{W}_2$ and $\hat{W}_3$ are associated with the λ_+, λ_{pv}, and λ_- waves respectively. Then from eq. (2.17)

$$\mathbf{Q}^{-1} = \begin{bmatrix} g & \bar{c}Y & \frac{f}{s}\bar{u} \\ \frac{\bar{u}g}{\bar{c}^2}\frac{f}{s} & \frac{f}{s} & 1 \\ g & -\bar{c}Y & \frac{f}{s}\bar{u} \end{bmatrix}, \tag{2.26}$$

and its inverse is

$$\mathbf{Q} = \left[2\bar{c}Y\left(1 - \frac{\bar{u}^2}{\bar{c}^2}\frac{f^2}{s^2}\right)\right]^{-1} \begin{bmatrix} \frac{\bar{c}}{g}(Y + \frac{\bar{u}}{\bar{c}}\frac{f^2}{s^2}) & -\frac{2\bar{u}\bar{c}Y}{g}\frac{f}{s} & \frac{\bar{c}}{g}(Y - \frac{\bar{u}}{\bar{c}}\frac{f^2}{s^2}) \\ 1 - \frac{\bar{u}^2}{\bar{c}^2}\frac{f^2}{s^2} & 0 & -1 + \frac{\bar{u}^2}{\bar{c}^2}\frac{f^2}{s^2} \\ -(1 + \frac{\bar{u}Y}{\bar{c}})\frac{f}{s} & 2\bar{c}Y & (1 - \frac{\bar{u}Y}{\bar{c}})\frac{f}{s} \end{bmatrix}. \tag{2.27}$$

Consider the boundary at $x = 0$. Let there be l values of $\lambda > 0$. Thus the host values of $\hat{W}^h_1, \hat{W}^h_2, ...\hat{W}^h_l$ must be imposed and the remaining values of $\hat{W}^g_{l+1}, ...\hat{W}^g_K$ must

be extrapolated from the interior, hence the superscript g, designating the nested 'guest' fields; $K = 3$, but the argument is quite general. Define

$$\hat{\mathbf{W}} = (\hat{W}_1^h, ...\hat{W}_l^h, \hat{W}_{l+1}^g, ...\hat{W}_K^g)^T, \tag{2.28}$$

then the boundary fields are given by

$$\hat{\mathbf{\Psi}} = \mathbf{Q}\hat{\mathbf{W}}. \tag{2.29}$$

Expand this as

$$\hat{\mathbf{\Psi}} = \mathbf{Q}^{(0)}\hat{\mathbf{W}}^{(0)} + \frac{f}{s}\Big(\mathbf{Q}^{(1)}\hat{\mathbf{W}}^{(0)} + \mathbf{Q}^{(0)}\hat{\mathbf{W}}^{(1)}\Big) + O\Big(\frac{f^2}{s^2}\Big), \tag{2.30}$$

where

$$\hat{\mathbf{W}}^{(i)} = [\mathbf{Q}^{-1}]^{(i)}\hat{\mathbf{\Psi}}. \tag{2.31}$$

The zero order matrices $\mathbf{Q}^{(0)}$ and $[\mathbf{Q}^{-1}]^{(0)}$ are defined by setting $f/s = 0$ in eqs. (2.26) and (2.27). Also, the first order matrices $\mathbf{Q}^{(1)}$ and $[\mathbf{Q}^{-1}]^{(1)}$ are defined by setting all except the terms proportional to f/s equal to zero. Dropping the $O(f^2/s^2)$ terms in eq. (2.30), multiplying by s, and transforming back yields the boundary fields

$$\frac{\partial \mathbf{\Psi}}{\partial t} = \mathbf{Q}^{(0)}\frac{\partial \mathbf{W}^{(0)}}{\partial t} + f\Big(\mathbf{Q}^{(1)}\mathbf{W}^{(0)} + \mathbf{Q}^{(0)}\mathbf{W}^{(1)}\Big). \tag{2.32}$$

The following simple discretization is used in the tests described later:

$$\Delta\mathbf{\Psi} = \mathbf{Q}^{(0)}\Delta\mathbf{W}^{(0)} + f\Delta t\Big(\mathbf{Q}^{(1)}\mathbf{W}_{av}^{(0)} + \mathbf{Q}^{(0)}\mathbf{W}_{av}^{(1)}\Big), \tag{2.33}$$

where for any field ϕ, $\Delta\phi = \phi^{n+1} - \phi^n$ and $\phi_{av} = (\phi^{n+1} + \phi^n)/2$.

In this derivation it has been assumed that it is permissible to regard f/s as a small parameter. Engquist and Majda (1977) furnish the theoretical justification. For an update, see Hagstrom (1999).

Remark: McDonald (2002) proposed that for $\bar{c} > \bar{u} > 0$, $g\eta + \bar{c}u$ and v be imposed at $x = 0$ for a two dimensional barotropic model. This corresponds to dropping the first order terms in eq. (2.30). From the point of view of this section, his boundary conditions are zero order for incoming waves and first order for outgoing waves. Notice however, that from a meteorological point of view, where the potential vorticity wave dominates, the

effective level of accuracy of the incoming waves may be almost first order for the following reason. In the absence of gravity waves $\mathbf{l}_+.\hat{\mathbf{\Psi}} = \mathbf{l}_-.\hat{\mathbf{\Psi}} = 0$, implying $g\hat{\eta} + (f\bar{u}\hat{v}/s) = 0$ and $\hat{u} = 0$, which when substituted in eq. (2.25) yields

$$\hat{W}_{pv} \equiv \hat{W}_2 = \hat{v}\Big(1 - \frac{f^2}{s^2}\frac{\bar{u}^2}{\bar{c}^2}\Big). \tag{2.34}$$

Hence, in the absence of gravity waves, imposing v at inflow is a first order condition. Of course, this argument breaks down if the guest model fields, or the host model fields which are being used to drive the guest model, contain large amplitude gravity waves.

2.3 Extrapolations associated with the boundary conditions

A grid is used in which the u-fields are staggered from the η-fields and v-fields, with both the latter at the end points. The boundary conditions are imposed at $x = \Delta x/2$ and $x = L - \Delta x/2$, rather than at 0 and L in order to minimize extrapolations. The details are given for imposing the boundary conditions at $x = \Delta x/2$ only. Exactly the same logic applies at $x = L - \Delta x/2$.

The following are used for computing $\mathbf{W}^g$ at time level $n+1$. The fields η and v are extrapolated; $u(\Delta x/2, n+1)$ is a known quantity:

$$\Psi_1(\frac{\Delta x}{2}, n+1) = 0.5[3\eta(\Delta x, n+1) - \eta(2\Delta x, n+1)];$$
$$\Psi_2(\frac{\Delta x}{2}, n+1) = u(\frac{\Delta x}{2}, n+1);$$
$$\Psi_3(\frac{\Delta x}{2}, n+1) = 0.5[3v(\Delta x, n+1) - v(2\Delta x, n+1)]. \tag{2.35}$$

The following are used for computing $\mathbf{W}^g$ at time level n and for computing $\mathbf{W}^h$ at time levels n and $n+1$.

$$\Psi_1(\frac{\Delta x}{2}, n) = 0.5[\eta(0, n) + \eta(\Delta x, n)];$$
$$\Psi_2(\frac{\Delta x}{2}, n) = u(\frac{\Delta x}{2}, n);$$
$$\Psi_3(\frac{\Delta x}{2}, n) = 0.5[v(0, n) + v(\Delta x, n)]. \tag{2.36}$$

Finally, once $\mathbf{\Psi}(\Delta x/2, n+1)$ has been re-constituted as a combination of interior and exterior fields, via eq. (2.29), η and v are then extrapolated to the boundary:

$$\Psi_m(0, n+1) = 2\Psi_m(\frac{\Delta x}{2}, n+1) - \Psi_m(\Delta x, n+1), \tag{2.37}$$

for $m = 1$ and 3.

2.4 Discretization of the equations of motion

For the spatial discretization the u-fields are staggered from the η- and v-fields, with both the latter at the end points. For the time discretization the leapfrog scheme is used. Thus, eqs. (2.1)-(2.3) are discretized as

$$\eta(i,n+1) = \eta(i,n-1) - \frac{\bar{u}\Delta t}{\Delta x}\Big[\eta(i+1,n) - \eta(i-1,n)\Big] - \frac{2H\Delta t}{\Delta x}\Big[u(i+\frac{1}{2},n) - u(i-\frac{1}{2},n)\Big], \tag{2.38}$$

$$u(i+\frac{1}{2},n+1) = u(i+\frac{1}{2},n-1) - \frac{\bar{u}\Delta t}{\Delta x}\Big[u(i+\frac{3}{2},n) - u(i-\frac{1}{2},n)\Big] - \frac{2g\Delta t}{\Delta x}\Big[\eta(i+1,n) - \eta(i,n)\Big] + f\Delta t\Big[v(i+1,n) + v(i,n)\Big], \tag{2.39}$$

$$v(i,n+1) = v(i,n-1) - \frac{\bar{u}\Delta t}{\Delta x}\Big[v(i+1,n) - v(i-1,n)\Big] - f\Delta t\Big[u(i+\frac{1}{2},n) + u(i-\frac{1}{2},n)\Big]. \tag{2.40}$$

where $x = i\Delta x, L = I\Delta x$, and $t = n\Delta t$. The boundary fields, $\eta(0,n+1), v(0,n+1), \eta(I,n+1)$, and $v(I,n+1)$, must be supplied. How to do this was discussed in sections 2.2 and 2.3. A Robert (1966) filter is used to control the computational mode. Equations (2.38) and (2.40) are valid from $i = 1$ to $i = I - 1$. Equation (2.39) is valid from $i = 0$ (where a right derivative is used for the advection term) to $i = I-1$ (where a left derivative is used for the advection term).

2.5 Testing the boundary conditions

In this section a practical demonstration is given of a potential vorticity wave being injected into the integration area while simultaneously two inertia-gravity waves radiate through the boundaries.

The parameters used were $\Delta x = 10$ km, $\Delta t = 9.0$ s, $\bar{u} = 50$ ms^{-1}, $gH = 300 \times 300$ m^{2}s^{-2}. These result in $\bar{c} = 300$ ms^{-1}. Thus the two gravity inertia waves have velocities of approximately 350 ms^{-1} and -250 ms^{-1}, typical of 'external' gravity waves, and the incoming potential vorticity wave is 'jet-like'.

Two sets of integrations were performed; one with $L = 1000$ km, $I = 101$, and a second 'host integration' with $L^h = 10000$ km, and $I^h = 1001$. The latter integration,

whose boundaries are so far removed that no waves can travel to them and back to the boundary of the guest integration domain during the length of the integration, was used as the 'correct integration' with which the test integrations were compared. It was also used to furnish the boundary fields to inject the potential vorticity wave into the region of integration. The first order boundary condition described by eq. (2.33) was used.

Defining a bell-shape as

$$b_i(x, x_s, \bar{c}_i^0 t, \Gamma_s) = exp\Big[-\Big\{\frac{(x - x_s - \bar{c}_i^0 t)}{\Gamma_s}\Big\}^2\Big], \tag{2.41}$$

where $\bar{\mathbf{c}}^0 = [\bar{u} + \bar{c}, \bar{u}, \bar{u} - \bar{c}]$, the initial state, which is displayed in Fig. 1, is given by

$$\begin{aligned}
\eta(x,0) &= \Big[\breve{Q}_{1,1}^{(0)}\frac{\partial b_1}{\partial t} + \breve{Q}_{1,3}^{(0)}\frac{\partial b_3}{\partial t}\Big]\Big(x, \frac{L}{2}, 0, \frac{L}{10}\Big) + \Big[\breve{Q}_{1,2}^{(1)} f b_2\Big]\Big(x, -\frac{L}{8}, 0, \frac{L}{10}\Big),\\
u(x,0) &= \Big[\breve{Q}_{2,1}^{(0)}\frac{\partial b_1}{\partial t} + \breve{Q}_{2,3}^{(0)}\frac{\partial b_3}{\partial t}\Big]\Big(x, \frac{L}{2}, 0, \frac{L}{10}\Big) + \Big[\breve{Q}_{2,2}^{(1)} f b_2\Big]\Big(x, -\frac{L}{8}, 0, \frac{L}{10}\Big),\\
v(x,0) &= \Big[\breve{Q}_{3,1}^{(1)} f b_1 + \breve{Q}_{3,3}^{(1)} f b_3\Big]\Big(x, \frac{L}{2}, 0, \frac{L}{10}\Big) + \Big[\breve{Q}_{3,2}^{(0)}\frac{\partial b_2}{\partial t}\Big]\Big(x, -\frac{L}{8}, 0, \frac{L}{10}\Big),
\end{aligned} \tag{2.42}$$

where $\breve{Q}_{i,j} = n_j Q_{i,j}$. The potential vorticity wave, for example, in eq. (2.42) is derived by putting $\hat{\mathbf{W}} = (0, s\hat{b}_2, 0)^T$ in eq. (2.29), dropping terms of higher order than f/s, and performing the inverse Laplace transform. The normalizations n_j were chosen such that the maximum value of η was equal to 10 m both for the shape centered at $x = L/2$ and for the shape centered at at $x = -L/8$. The host initial state was

$$\begin{aligned}
\eta(x^h,0) &= \breve{Q}_{1,2}^{(1)} f b_2\Big(x^h, \frac{L^h}{2} - \frac{L}{2} - \frac{L}{8}, 0, \frac{L}{10}\Big),\\
u(x^h,0) &= \breve{Q}_{2,2}^{(1)} f b_2\Big(x^h, \frac{L^h}{2} - \frac{L}{2} - \frac{L}{8}, 0, \frac{L}{10}\Big),\\
v(x^h,0) &= \breve{Q}_{3,2}^{(0)}\frac{\partial b_2}{\partial t}\Big(x^h, \frac{L^h}{2} - \frac{L}{2} - \frac{L}{8}, 0, \frac{L}{10}\Big);
\end{aligned} \tag{2.43}$$

($x^h = L^h/2$ is the same point in space as $x = L/2$).

Once the integration starts the λ_+-wave will travel toward the boundary at $x = L$ at an approximate velocity of $\bar{u}+\bar{c}$, the λ_--wave will travel toward the boundary at $x = 0$ at an approximate velocity of $\bar{u} - \bar{c}$; simultaneously the λ_{pv}-wave will enter through the boundary at $x = 0$ at an approximate velocity $\bar{u}$. The situation after 22.5 mins is displayed in Fig. 2. As can be seen, the centre of the two inertia-gravity waves are at approximately

973 km and 163 km as they should be, and the potential vorticity wave has progressed into the area. (These waves will eventually disperse, but they remain recognizable for quite some time). The integration after 167 mins, at which time the incoming potential vorticity wave has travelled approximately 500 km, is shown in Fig. 3. Notice the two gravity inertia waves have exited without reflection and to the eye the potential vorticity wave has entered the area without distortion and its centre is at 375 km, as it should be. A quantitative measure of the transparency of the boundaries is the fact that the maximum rms error for η using the host model forecast as the 'correct answer' is 0.001 m. For comparison, a repeat of this forecast using the boundary conditions $\eta = u = v = 0$, which reflect the inertia gravity waves and prevent the potential vorticity wave from entering gives a maximum rms error for η of ~ 3 m. Using these numbers it is fair to argue that the boundaries are more than 99.9% transparent to the incoming potential vorticity wave.

Caveat. It is essential that at $t = 0$ the initial and boundary fields agree. A discontinuity at $x = 0$ will cause η, u and v to drift to unphysical values as the integration proceeds. For example, if the integration described above is repeated with exactly the same boundary conditions and the same initial state *except* for the absence of the tail of the encroaching bell seen at the left hand edge of of Fig. 1, the outcome will be radically different. The introduced discontinuity causes the values of η, u, and v to drift to totally unphysical values. (The boundary conditions are 'working' in the sense that the potential vorticity field defined by eq. (2.24) enters the area exactly as it should, and the two fields '$\partial(g\eta \pm \bar{u})/\partial t + fv$' exit the area as they should. However they are not working in that the undifferentiated fields η, u, and v drift away to unphysical values).

3. A two layer model

The purpose of this section is (a) to derive transparent boundary conditions for the simplest possible system of linear equations which supports baroclinic waves as well as barotropic and potential vorticity waves; (b) to demonstrate via a practical integration that potential vorticity can be injected accurately into the integration area while simultaneously allowing baroclinic gravity inertia waves and potential vorticity waves to exit without reflection.

The system of equations which describes two superposed immiscible fluids of different density are derived from the conservation of mass and momentum in the presence of the Coriolis force by Gill, 1982, for example. The equations are

$$\frac{\partial \eta_1}{\partial t} + \bar{u}\frac{\partial \eta_1}{\partial x} + H_1\frac{\partial u_1}{\partial x} + H_2\frac{\partial u_2}{\partial x} = 0, \tag{3.1}$$

$$\frac{\partial \eta_2}{\partial t} + \bar{u}\frac{\partial \eta_2}{\partial x} + H_2\frac{\partial u_2}{\partial x} = 0, \tag{3.2}$$

$$\frac{\partial u_1}{\partial t} + \bar{u}\frac{\partial u_1}{\partial x} + g\frac{\partial \eta_1}{\partial x} - fv_1 = 0, \tag{3.3}$$

$$\frac{\partial u_2}{\partial t} + \bar{u}\frac{\partial u_2}{\partial x} + g''\frac{\partial \eta_1}{\partial x} + g'\frac{\partial \eta_2}{\partial x} - fv_2 = 0, \tag{3.4}$$

$$\frac{\partial v_1}{\partial t} + \bar{u}\frac{\partial v_1}{\partial x} + fu_1 = 0, \tag{3.5}$$

$$\frac{\partial v_2}{\partial t} + \bar{u}\frac{\partial v_2}{\partial x} + fu_2 = 0, \tag{3.6}$$

Here

$$g'' = g\frac{\rho_1}{\rho_2}; \qquad g' = g\left(1 - \frac{\rho_1}{\rho_2}\right); \tag{3.7}$$

where ρ_1 and ρ_2 are the densities of the upper and lower fluids, respectively. The fields $\eta_1(x,t)$ and $\eta_2(x,t)$ describe the displacement of the fluid surfaces from their resting thicknesses, H_1 and H_2, respectively. Lastly, $u_1(x,t)$ and $u_2(x,t)$ are the eastward horizontal velocity components and $v_1(x,t)$ and $v_2(x,t)$ are the northward horizontal velocity components. See Fig. 6.1 of Gill (1982).

Let $\mathbf{\Psi}$ be the vector

$$\mathbf{\Psi} = (\eta_1, \eta_2, u_1, u_2, v_1, v_2)^T. \tag{3.8}$$

Then the derivation of the boundary conditions is exactly the same as in section 2, but now with new 6×6 matrices $\mathbf{A}$ and $\mathbf{B}$, which are tabulated in appendix A, as are the eigenvalues and left eigenvectors.

There is a puzzling question about the eigenvectors associated with the eigenvalues λ_3 and λ_4. Because they are equal, see eq. (A10), it is legitimate to choose any two left eigenvectors which are linearly independent. Thus, $\mathbf{l}_3$ and $\mathbf{l}_4$ of eq. (A11) are not unique; nor has this combination been chosen for any particular reason. Any other two linearly independent combination of these two eigenvectors could equally well be used. It is an

open question whether a particular combination is 'best' in some sense, such as making the mathematics simpler, or improving our intuitive understanding.

For the λ_3- and λ_4-waves the zero order solution is dominated by v_1 and v_2:

$$v_1(x,t) = v_1\Big(x_0, t - \frac{x-x_0}{\bar{u}}\Big) + In_3^{(0)},$$
$$v_2(x,t) = v_2\Big(x_0, t - \frac{x-x_0}{\bar{u}}\Big) + In_4^{(0)}, \tag{3.9}$$

and the first order solutions are

$$\Big[\frac{\partial v_1}{\partial t} + fu_1 + \frac{f\bar{u}}{H_1}\Big(\eta_1 - \eta_2\Big)\Big](x,t) = \Big[\frac{\partial v_1}{\partial t} + fu_1 + \frac{f\bar{u}}{H_1}\Big(\eta_1 - \eta_2\Big)\Big]\Big(x_0, t - \frac{x-x_0}{\bar{u}}\Big), \tag{3.10}$$

and

$$\Big[\frac{\partial v_2}{\partial t} + fu_2 + \frac{f\bar{u}}{H_2}\eta_2\Big](x,t) = \Big[\frac{\partial v_2}{\partial t} + fu_2 + \frac{f\bar{u}}{H_2}\eta_2\Big]\Big(x_0, t - \frac{x-x_0}{\bar{u}}\Big); \tag{3.11}$$

see eq. (A11).

Substituting u_1 from eq. (3.5) in eq. (3.10) and u_2 from eq. (3.6) in eq. (3.11) yields

$$-\frac{1}{\bar{u}}\Big[\frac{\partial v_1}{\partial t} + fu_1 + \frac{f\bar{u}}{H_1}\Big(\eta_1 - \eta_2\Big)\Big] = \frac{\partial v_1}{\partial x} - \frac{f}{H_1}(\eta_1 - \eta_2), \tag{3.12}$$

and

$$-\frac{1}{\bar{u}}\Big[\frac{\partial v_2}{\partial t} + fu_2 + \frac{f\bar{u}}{H_2}\eta_2\Big] = \frac{\partial v_2}{\partial x} - \frac{f}{H_2}\eta_2, \tag{3.13}$$

the potential vorticity for the system of equations (3.1)-(3.6). That these quantities are conserved following the parcel can be seen by taking $\partial/\partial x$ of eq. (3.5) and subtracting f/H_1 times [eq. (3.1) minus eq. (3.2)] for the former and by taking $\partial/\partial x$ of eq. (3.6) and subtracting f/H_2 times eq. (3.2) for the latter.

Now, as was argued above, if $\bar{u} > 0$, in a nested integration, in order to inject potential vorticity into the integration at $x = 0$ via a host model put $v_1(t,0) = v_1^h(t,0)$ and $v_2(t,0) = v_2^h(t,0)$ to lowest order. To all higher orders put $[\partial v_2/\partial t + fu_2 + f\bar{u}\eta_2/H_2](0,t)$ and $[\partial v_1/\partial t + fu_1 + f\bar{u}(\eta_1 - \eta_2)/H_1](0,t)$ equal to their host model values. If $\bar{u} < 0$ the reasoning is the same except that it applies to the boundary at $x = L$.

In practice the boundary conditions are not implemented in exactly this way, but rather, in an order consistent fashion as described in section 2.2. The requisite matrices $\mathbf{Q}^{(0)}, \mathbf{Q}^{(1)}$, etc. are tabulated in Appendix A.

Notice that the first four terms of $\mathbf{l}_1^{(1)}$ of eq. (A11) with $f/s = 0$ and row 1 of $\mathbf{Q}^{-1}$ in eq. (2.17) of M05 are identical ($c_0^2 c_1^2 = gg' H_1 H_2$). Thus, a pattern is emerging for the gravity inertia waves which arises again in the multi-level model described in section 3. The lowest order solution is exactly that of M05. The first order boundary field derived from the inverse transform of $\mathbf{l}_1.\hat{\mathbf{\Psi}}$ using $\mathbf{l}_1$ from eq. (A11) with $n_1(s) = s$,

$$\frac{\partial}{\partial t}\left[a_1\eta_1 - \eta_2 + \frac{H_1 a_1}{c_0}u_1 - \frac{c_0}{g'}u_2\right] + \frac{f\bar{u}H_1 a_1}{c_0^2}v_1 - \frac{f\bar{u}}{g'}v_2, \tag{3.14}$$

has the same structure as eq. (2.21): it is a combination of the time derivative of the characteristic combination of the fields with $f\bar{u}$ times a combination of v-terms. For the other gravity-inertia waves, associated with the eigenvalues λ_2, λ_5, and λ_6 of eq. A11, the same structure is present.

3.1 Testing the boundary conditions

In this section a practical demonstration is given of a potential vorticity wave being injected into the integration area while barotropic and baroclinic waves simultaneously exit the area.

The same method of spatial and temporal discretization was used for eqs. (3.1)-(3.6) as was used for eqs. (2.1)-(2.3); see section 2.4 . The boundary conditions are those given by eq. (2.33), but using the vectors and matrices defined in Appendix A.

The parameters are $\Delta x = 10$ km, $\Delta t = 9.0$ s, $g' = 4.09$, $g'' = 5.72$, $H_1 = 5000$ m, $H_2 = 5000$ m, $\bar{u} = 50$ ms^{-1}. These result in $c_0 = 294.1$ ms^{-1} and $c_1 = 107.6$ ms^{-1}. The values of g' and g'' result from using the ICAO densities at 7500 m ($\rho_1 = 0.56$ kgm^{-3}) and 2500 m ($\rho_2 = 0.96$ kgm^{-3}). As previously, two sets of integrations were performed; one with $L = 1000$ km, $I = 101$, and a second host integration with $L^h = 10000$ km, and $I^h = 1001$, and the output of the latter was used to furnish the data for the incoming potential vorticity wave and also to compute the rms errors.

The initial state consisted of a bell-shape distortion of the two surfaces centered at $L/2$ whose amplitude was 10m; see Fig. 4 . The bell-shape is defined as in eq. (2.41),

but with $\bar{\mathbf{c}}^0 = [\bar{u}+\bar{c}_0, \bar{u}+\bar{c}_1, \bar{u}, \bar{u}, \bar{u}-\bar{c}_1, \bar{u}-\bar{c}_0]$,

$$\eta_1(x,0) = 10\ b_1(x, L/2, 0, L/20); \quad \eta_2(x,0) = -\eta_1(x,0); \quad u_1(x,0) = 0; \quad u_2(x,0) = 0. \tag{3.15}$$

For the 'host integration' initial state $L^h/2$ replaces $L/2$ in eq. (3.15) plus there was a λ_3-wave of amplitude 10m situated at $L^h/2 - 3L/4$:

$$\Psi_m(x,0) = \frac{10}{Q^{(1)}_{1,3}}\left[Q^{(1)}_{m,3} b_3 + \frac{1}{f} Q^{(0)}_{m,3} \frac{\partial b_3}{\partial t}\right]\left(x^h, \frac{L^h}{2} - \frac{3L}{4}, 0, \frac{L}{20}\right) \tag{3.16}$$

For such an initial state, if $\bar{c}_0 > \bar{c}_1 > \bar{u} > 0$, then once the integration starts a λ_1- and λ_2-wave will travel in the $+x$-direction with approximate velocities $\bar{u}+c_0$ and $\bar{u}+c_1$, respectively; a λ_5 and λ_6-wave will travel in the $-x$-direction with approximate velocities $\bar{u}-c_1$ and $\bar{u}-c_0$, respectively; simultaneously the λ_3-wave will enter through the boundary at $x=0$ at a velocity $\bar{u}$ approximately at the same time as the λ_5 wave exits. These bell-shapes will gradually disperse as the integration proceeds, because of the presence of the Coriolis terms, but they will remain recognizable for a reasonable period; see Fig. 5.

The eigenvalues $\lambda_1, \lambda_2, \lambda_3$, and λ_4 are greater than zero. Thus, in generating the boundary conditions using eqs. (2.28) and (2.92), four $\hat{W}^h$'s and two $\hat{W}^g$'s were required at $x=0$, and two $\hat{W}^h$'s and four $\hat{W}^g$'s at $x=L$. To generate the W^h's needed for eq. (2.33) the field $\mathbf{\Psi}^h(x^h = L^h/2 - L/2 + \Delta x/2)$ was computed at every time step of the host integration and written to a file. During the nested guest integration this field was read in at each time step and used to generate the externally supplied boundary field $\hat{W}^h_3(\Delta x/2, n+1)$ in eq. (2.28).

In Fig. 5 is plotted the values of the height fields after 250 mins, at which time the apex of the λ_3-wave would be situated at $x = 500$ km in the absence of dispersion, whose presence causes the original bell shape to develop the tail seen in Fig. 5, from which one can argue that the two gravity waves have exited stably and without visible reflection, while the potential vorticity wave has visibly entered the integration region. A quantitative measure is give by the rms error. After 250 mins it was 0.042 m for η_1 and 0.111 m for η_2. To measure the relative accuracy the forecast was repeated with all the fields set to zero on the boundary, causing the gravity inertia waves to be reflected and preventing the potential vorticity waves from entering. Then after 250 mins the rms error

was 2.92 m for η_1 and 4.36 m for η_2. By this measure the boundaries cause a 1.4% error in η_1 and a 2.5% error in η_2.

It is reasonable to conclude that this approach to handling the open boundary problem can simultaneously handle potential vorticity, barotropic, and baroclinic waves. This inspires the confidence to take the next step, that is, to tackle a more realistic multi-level model.

4. A multi-level model

In this section (semi)-transparent boundary conditions are derived for a system of equations which supports multiple baroclinic and potential vorticity waves: the two dimensional linearized hydrostatic primitive equations. A practical demonstration is given of their transparency.

4.1 The equations and their vertical discretization

Gill (1982) gives a description of the approximations involved in arriving at the following linearized set of equations. See section 7.12 of his book for a discussion of their analytical solutions. The following are his equations 7.12.1, 7.12.2, 6.4.6, 6.11.2, and 6.4.3, respectively, with $\partial/\partial y = 0$.

$$\frac{du'(x,z,t)}{dt} + \frac{1}{\rho_0(z)}\frac{\partial p'(x,z,t)}{\partial x} - fv'(x,z,t) = 0, \tag{4.1}$$

$$\frac{dv'(x,z,t)}{dt} + fu'(x,z,t) = 0, \tag{4.2}$$

$$\frac{d\rho'(x,z,t)}{dt} + \frac{d\rho_0(z)}{dz}w'(x,z,t) = 0, \tag{4.3}$$

$$\frac{\partial p'(x,z,t)}{dz} + g\rho'(x,z,t) = 0, \tag{4.4}$$

$$\frac{\partial u'(x,z,t)}{\partial x} + \frac{\partial w'(x,z,t)}{\partial z} = 0. \tag{4.5}$$

In these equations the pressure p', the density ρ', and the x-, y-, and z- components of the winds u', v', and w' are small deviations from an isothermal atmosphere, whose fields

are designated by the subscript zero and whose density is $\rho_0(z)$. Lastly,

$$\frac{d}{dt} = \frac{\partial}{\partial t} + u_0 \frac{\partial}{\partial x}, \tag{4.6}$$

where u_0 is a constant.

Discretizing in the vertical and defining the ρ'-, u'- and v'- fields on the 'full' levels, and the p'- and w'- fields on the 'half' levels gives rise to the following set of equations.

$$\frac{du_m(x,t)}{dt} + \frac{\partial p_m(x,t)}{\partial x} - f v_m(x,t) = 0; \qquad m = 1, M, \tag{4.7}$$

$$\frac{dv_m(x,t)}{dt} + f u_m(x,t) = 0; \qquad m = 1, M, \tag{4.8}$$

$$\frac{\partial u_m(x,t)}{\partial x} + \frac{w_{m+\frac{1}{2}}(x,t) - w_{m-\frac{1}{2}}(x,t)}{\Delta z_m} + \frac{N_m^2}{g} w_m(x,t) = 0; \qquad m = 1, M, \tag{4.9}$$

$$\frac{d\rho_m(x,t)}{dt} - \frac{N_m^2}{g} w_m(x,t) = 0; \qquad m = 2, M, \tag{4.10}$$

$$\frac{p_{m+\frac{1}{2}}(x,t) - p_{m-\frac{1}{2}}(x,t)}{\Delta z_m} + g\rho_m(x,t) = 0; \qquad m = 2, M, \tag{4.11}$$

$$\frac{p_{\frac{3}{2}}(x,t) - p_{\frac{1}{2}}(x,t)}{\Delta z_1} + g\rho_2(x,t) = 0, \tag{4.12}$$

where the Brunt-Väisälä frequency, N^2, is defined in terms of the density of the isothermal atmosphere as

$$N^2(z) = -\frac{g}{\rho_0(z)} \frac{d\rho_0(z)}{dz}, \tag{4.13}$$

and to reduce typographical clutter later in this section, $p = p', \rho = \rho', u = \rho_0 u', v = \rho_0 v'$, and $w = \rho_0 w'$. The reason there is no ρ_1-field is to eliminate an unwanted computational mode. This is further discussed in section 4.3.

It is important to emphasize that p_m and w_m are defined by the average of the two adjacent half-levels:

$$p_m \equiv \frac{1}{2}[p_{m+\frac{1}{2}} + p_{m-\frac{1}{2}}]; \qquad w_m \equiv \frac{1}{2}[w_{m+\frac{1}{2}} + w_{m-\frac{1}{2}}]. \tag{4.14}$$

Also,

$$\Delta z_m \equiv z_{m+\frac{1}{2}} - z_{m-\frac{1}{2}}. \tag{4.15}$$

Finally, it is necessary to define boundary conditions at the *top* of the atmosphere, $z_{\frac{1}{2}}$, and at the *bottom* of the atmosphere, $z_{M+\frac{1}{2}}$, where M is the number of full levels. In the absence of orography the physical boundary condition at the bottom is

$$w_{M+\frac{1}{2}} = 0. \tag{4.16}$$

At the top of the atmosphere the boundary condition $w_{\frac{1}{2}} = 0$ kills the external mode; see Kalnay (2003), p 46 . Consequently, a material boundary is used at the top in order to retain this mode :

$$\frac{dp_{\frac{1}{2}}(x,t)}{dt} - gw_{\frac{1}{2}}(x,t) = 0. \tag{4.17}$$

Defining $a_m^{\pm} = [1 \pm \Delta z_m N_m^2/(2g)]$, multiplying eq. (4.9) by Δz_m, and summing over m yields a recursive relation for $w_{m-\frac{1}{2}}$:

$$w_{m-\frac{1}{2}}(x,t) = \frac{1}{a_m^-}\Big(\Delta z_m \frac{\partial u_m(x,t)}{\partial x} + a_m^+ w_{m+\frac{1}{2}}(x,t)\Big), \tag{4.18}$$

which, combined with the definition of w_m in eq. (4.14), facilitates the replacement of eq. (4.9) with the following two equations:

$$w_m(x,t) = -\frac{g}{N_m^2}\sum_{j=1}^{M} \tau_{m,j}\frac{\partial u_j(x,t)}{\partial x}, \tag{4.19}$$

$$w_{\frac{1}{2}}(x,t) = -\frac{1}{g}\sum_{j=1}^{M} \nu_j \frac{\partial u_j(x,t)}{\partial x}. \tag{4.20}$$

The matrix $\boldsymbol{\tau}$ and the transposed vector $\boldsymbol{\nu}$ are functions of $\Delta z, N^2$, and g only. Although algebraically complicated they are rather easy to generate in a computer program because of their recursiveness. The factors in front of eqs. (4.19) and (4.20) are included to make eqs. (4.30) and (4.31) look more elegant.

Multiplying eq. (4.12) by Δz_1 and using the definition of p_m in eq. (4.14) yields

$$p_1 = p_{\frac{1}{2}} - g\frac{\Delta z_1}{2}\rho_2. \tag{4.21}$$

Multiplying eq. (4.11) by Δz_m and summing from the top down results in

$$p_m = p_{\frac{1}{2}} - g\Big(\frac{\Delta z_m}{2}\rho_m + \sum_{j=2}^{m-1}\Delta z_j\rho_j + \Delta z_1\rho_2\Big); \qquad m = 2, M \tag{4.22}$$

and

$$p_{M+\frac{1}{2}} = p_{\frac{1}{2}} - g\Big(\sum_{j=2}^{M} \Delta z_j \rho_j + \Delta z_1 \rho_2\Big). \tag{4.23}$$

If a field ρ_1 is defined such that

$$-g\Delta z_1 \rho_1 = p_{\frac{1}{2}} - g\Delta z_1 \rho_2, \tag{4.24}$$

then eqs. (4.21)-(4.23) can be written as

$$\mathbf{p} = \mathbf{\Gamma}\boldsymbol{\rho} \ , \tag{4.25}$$

$$p_{M+\frac{1}{2}} = \boldsymbol{\eta}\boldsymbol{\cdot}\boldsymbol{\rho} \ , \tag{4.26}$$

where $\mathbf{\Gamma}$ is a square matrix defined by the relationships

$$p_1 = -g\Delta z_1(\rho_1 - \frac{1}{2}\rho_2), \tag{4.27}$$

$$p_m = -g\Big(\frac{\Delta z_m}{2}\rho_m + \sum_{j=1}^{m-1} \Delta z_j \rho_j\Big); \qquad m = 2, M, \tag{4.28}$$

and $\boldsymbol{\eta}$ is a transposed vector defined by

$$p_{M+\frac{1}{2}} = -g\sum_{j=1}^{M} \Delta z_j \rho_j. \tag{4.29}$$

It is important to emphasize that ρ_1 is *not* the density at level 1. The reason for its introduction is to restructure eqs. (4.21)-(4.23) into a form which lends itself to formal matrix manipulation.

Using these matrices the equations (4.10) and (4.17) can be written as

$$\frac{d\rho_m(x,t)}{dt} + \sum_{j=1}^{M} \tau_{m,j} \frac{\partial u_j(x,t)}{\partial x} = 0; \qquad m = 2, M, \tag{4.30}$$

and

$$\frac{dp_{\frac{1}{2}}(x,t)}{dt} + \boldsymbol{\nu}\boldsymbol{\cdot}\frac{\partial \mathbf{u}(x,t)}{\partial x} = 0. \tag{4.31}$$

To solve the equations of motion in the interior eqs. (4.7), (4.8), (4.30), and (4.31) are used to update u_m and v_m for $m = 1, M$, ρ_m for $m = 2, M$, and $p_{\frac{1}{2}}$, respectively. Then eq. (4.24) is used to get ρ_1, which is then used in eq. (4.25) to update $\mathbf{p}$.

4.2 The lateral boundary conditions

To derive the lateral boundary conditions one proceeds as follows. Take d/dt of eq. (4.24) and substitute the resulting $dp_{\frac{1}{2}}/dt$ in eq. (4.31). Combining the result with eq. (4.30) one arrives at the equation

$$\frac{d\boldsymbol{\rho}\ (x,t)}{dt} + \check{\boldsymbol{\tau}}\ \frac{\partial \mathbf{u}(x,t)}{\partial x} = 0, \tag{4.32}$$

where for any vector $\mathbf{D} = (D_1, D_2, ...D_M)^T$,

$$(\check{\boldsymbol{\tau}}\boldsymbol{D})_1 = (\boldsymbol{\tau}\boldsymbol{D})_2 - \frac{1}{g\Delta z_1}\boldsymbol{\nu}.\boldsymbol{D}; \quad (\check{\boldsymbol{\tau}}\boldsymbol{D})_m \equiv (\boldsymbol{\tau}\boldsymbol{D})_m, \quad m = 2, M. \tag{4.33}$$

Taking d/dt of eq. (4.25) and substituting the result in $\boldsymbol{\Gamma}$ times eq. (4.32) results in

$$\frac{d\mathbf{p}(x,t)}{dt} + \boldsymbol{\Gamma}\check{\boldsymbol{\tau}}\ \frac{\partial \mathbf{u}(x,t)}{\partial x} = 0. \tag{4.34}$$

Assume there exists a matrix $\mathbf{E}$ which diagonalizes $\boldsymbol{\Gamma}\check{\boldsymbol{\tau}}$:

$$\mathbf{E}^{-1}\boldsymbol{\Gamma}\check{\boldsymbol{\tau}}\boldsymbol{E}\ = \mathbf{C^2}, \tag{4.35}$$

where the diagonal matrix has been written as $\mathbf{C^2}$ for later convenience. The diagonal elements are defined as $C_{m,m} = c_m$. Using eq. (4.35), eqs. (4.34), (4.7), and (4.8) can be re-written as

$$\frac{d(\mathbf{E^{-1}p})_m}{dt} + c_m^2 \frac{\partial(\mathbf{E^{-1}u})_m}{\partial x} = 0, \tag{4.36}$$

$$\frac{d(\mathbf{E^{-1}u})_m}{dt} + \frac{\partial(\mathbf{E^{-1}p})_m}{\partial x} - f(\mathbf{E^{-1}v})_m = 0, \tag{4.37}$$

$$\frac{d(\mathbf{E^{-1}v})_m}{dt} + f(\mathbf{E^{-1}u})_m = 0. \tag{4.38}$$

For each $m = 1, M$ eqs. (4.36)-(4.38) are formally identical to eqs. (2.1)-(2.3). Therefore the method derived for generating the semi-transparent boundary fields in section 2 can be applied to derive $\mathbf{E^{-1}p}, \mathbf{E^{-1}u}$ and $\mathbf{E^{-1}v}$ at the boundaries, from which $\mathbf{u}, \mathbf{v}$, and $\mathbf{p}$ at the boundaries follow trivially. Thereafter $\boldsymbol{\rho}$ at the boundary is derived by operating on eq. (4.25) with $\boldsymbol{\Gamma}^{-1}$, which, in turn allows the computation of the boundary values of $p_{\frac{1}{2}}$ via eq. (4.24).

4.3 The vertical distribution of the fields

The purpose of this section is to answer the question: why the inelegant choice of having no ρ_1-field in eqs. (4.10)-(4.12)? To answer this consider what would have happened if this field had been retained. Using the same derivation as in section 4.1, then instead of eq. (4.25), the following relationship between $\mathbf{p}$ and $\boldsymbol{\rho}$ would have resulted:

$$p_m = p_{\frac{1}{2}} - g\Big(\frac{\Delta z_m}{2}\rho_m + \sum_{j=1}^{m-1} \Delta z_j \rho_j\Big); \tag{4.39}$$

see eqs. (3.22) and (3.23) of M05. Also, instead of eq. (4.34) the following equation would have been derived:

$$\frac{d\mathbf{p}(x,t)}{dt} + \mathbf{M}\frac{\partial \mathbf{u}(x,t)}{\partial x} = 0, \tag{4.40}$$

where the $M \times M$ matrix $\mathbf{M}$ is defined in M05. We then would have proceeded as described in section 4.2 to derive semi-transparent boundary conditions for the $3 \times M$ fields $\mathbf{u}, \mathbf{v}$ and $\mathbf{p}$. Now there would be a problem: $M+1$ boundary fields, $(\rho_m, m = 1, M,\ and\ \ p_{\frac{1}{2}})$ would be needed in order to continue with the integration, but there are only M values of $\mathbf{p}$ available for their computation. That is, eq. (4.39) could not be inverted because it is under determined.

This is a well-known problem associated with this vertical distribution of the fields, and normally some physical assumption, which is not appropriate for deriving transparent boundary conditions, is made to provide the extra piece of information. See, for example 'step c' on page 108 of Daley (1979) for his physical assumption, made in the context of normal mode initialization.

Looking at eq. (4.39), it will become invertible if any one of the ρ_m fields is removed. If this is done one arrives at a relation, such as eq. (4.25), which can be solved for $\boldsymbol{\rho}$ without any additional assumptions. Equation (4.24) then yields $p_{\frac{1}{2}}$. (The choice of removing ρ_1 was made on the basis of mathematical convenience, see eq. (4.33), and physical reasoning: if two layers of the model must have the same density anomaly, then in a meteorological model the top two layers are almost certainly the best choice).

One may ask the question: how was this problem avoided in M05? The answer is that for the gravity waves there is an additional condition, which can be seen by writing

eq. (A9) of M05 in the more elegant form

$$\frac{d}{dt}\Big(\boldsymbol{\tau}^{-1}\boldsymbol{\rho} - \mathbf{M}^{-1}\mathbf{p}\Big) = 0, \tag{4.41}$$

which permits the computation of $\boldsymbol{\rho}$ if $\mathbf{p}$ is known:

$$\boldsymbol{\rho} = \boldsymbol{\tau}\ \mathbf{M}^{-1}\mathbf{p}. \tag{4.42}$$

However, when the Coriolis terms are included there is a subtle change: the equations now support additional solutions: the potential vorticity waves. They have the property that $d\psi/dt = 0$ for any field ψ. As a result, eq. (4.41), which still holds when the Coriolis terms are present, no longer gives an additional relationship between $\boldsymbol{\rho}$ and $\mathbf{p}$.

4.4 Testing the boundary conditions

In this section a practical demonstration is given of the transparency of the boundary conditions derived in section 4.2. First, it is shown that the boundary conditions work well for outgoing potential vorticity waves. Second, it is shown that they are transparent to an externally imposed incoming potential vorticity wave: it enters almost without distortion. Lastly, it is shown that the slowest gravity wave, for which $u_0/\bar{c} \approx 10$ and thus for which the assumption that f^2/s^2 can be regarded as a small quantity is under the most strain (see eq. (2.15)), exits the area with minimal reflection.

The horizontal spatial discretization of eqs. (4.7), (4.8), (4.30), and (4.31) is the same as that for eqs. (2.38)-(2.40) with the fields ρ_m, p_m and $p_{\frac{1}{2}}$ being discretized as are the η fields there. A Robert (1966) filter is used to control the computational mode.

For an isothermal atmosphere $N^2 = g^2/(RT_0)$. The value $T_0 = 250$ K was used; $R = 287.04$ J kg^{-1} K^{-1}. For the discretization, $\Delta x = 10$ km, $\Delta t = 9.0$ s, $z_{\frac{1}{2}} = 10$ km; $M = 10$ and the levels are equally spaced; thus $\Delta z_m = -1$ km. These result in $c_1 = 281.5$, $c_2 = 100.5$, $c_3 = 54.6$, $c_4 = 36.1$, $c_5 = 25.5$, $c_6 = 18.3$, $c_7 = 12.9$, $c_8 = 8.6$, $c_9 = 5.0$, $c_{10} = 1.6$, all of these having units of ms^{-1}. The impact of changing the treatment of the density in the top layer can be seen by comparing these velocities with those in M05. The advecting velocity was chosen to be $u_0 = 25$ ms^{-1}.

The matrices $\mathbf{Q_m^{-1}}$ and $\mathbf{Q_m}$ used in this section are defined by eqs. (2.26) and (2.27) respectively with $\bar{c}$ replaced by c_m and $\bar{u}$ replaced by u_0. Also, the gravity-inertia wave

solution whose velocity is $u_0 \pm c_m$ will be called the '$\{m\}_{\pm}$-wave', and the corresponding potential vorticity wave the '$\{m\}_{pv}$-wave'.

Two sets of integrations were performed; one with $L = 1000$ km, $I = 101$, and a second 'host integration' with $L^h = 10000$ km, and $I^h = 1001$. The latter integration furnished the correct forecast for measuring the errors for all three tests that follow and also the boundary fields describing and the incoming waves in test 2 below.

To measure the error for any field ψ, the root mean square difference between the fields ψ^n and $(\psi^h)^n$ was computed at each time step n. To measure the relative magnitude of this error it was divided by the root mean square difference between the $(\psi^h)^n$ and zero at time N:

$$R^n(\psi) = \left[\sum_{i=1}^{I}\sum_{k=1}^{M}\{(\psi^h)^n_{i,k} - \psi^n_{i,k}\}^2\right]^{\frac{1}{2}} \div \left[\sum_{i=1}^{I}\sum_{k=1}^{M}\{(\psi^h)^N_{i,k}\}^2\right]^{\frac{1}{2}}. \tag{4.43}$$

N differs from test to test because the denominator only makes sense in these tests when the 'shape' is inside the integration area and it will be chosen judiciously depending on the test being performed.

Test 1. Do the potential vorticity waves exit without reflection?

To see whether the potential vorticity waves exited without reflection the following pure $\{m\}_{pv}$-wave, centered at $L/2$, was used as an initial state:

$$\begin{aligned} p_j(x,0) &= E_{j,m}[\breve{Q}_m]^{(1)}_{1,2} fb_2\left(x, \frac{L}{2}, 0, \frac{L}{10}\right), \\ u_j(x,0) &= E_{j,m}[\breve{Q}_m]^{(1)}_{2,2} fb_2\left(x, \frac{L}{2}, 0, \frac{L}{10}\right), \\ v_j(x,0) &= E_{j,m}[\breve{Q}_m]^{(0)}_{3,2} \frac{\partial b_2}{\partial t}\left(x, \frac{L}{2}, 0, \frac{L}{10}\right), \end{aligned} \tag{4.44}$$

where $[\breve{Q}_m]_{i,2} = n_2[Q_m]_{i,2}$. The normalization n_2 was chosen such that the maximum value of $|v'_m(x,0)| = 10$ ms^{-1}. The $m = 5$ wave initial state is displayed in Fig. 6. Once the integration began this shape moved toward the boundary at $x = L$ with a velocity of 25 ms^{-1}. Because the shape is approximately 400 km wide, see Fig. 6, it took about 7.8 h for the bulk of it to clear the area; (700 km at 25 ms^{-1}).

In order to make this test meaningful the host model fields were used *solely* to measure the rms errors. Thus, in using eq. (2.28) the $\hat{\mathbf{W}}$ were chosen as follows for

each mode $m = 1, 5$: at $x = 0$, $\hat{\mathbf{W}} = (0, 0, \hat{W}_3^g)^T$ and at $x = L$, $\hat{\mathbf{W}} = (\hat{W}_1^g, \hat{W}_2^g, 0)^T$; and as follows for each mode $m = 6, 10$: at $x = 0$, $\hat{\mathbf{W}} = (0, 0, 0)^T$ and at $x = L$, $\hat{\mathbf{W}} = (\hat{W}_1^g, \hat{W}_2^g, \hat{W}_3^g)^T$.

The error caused by any reflection at $x = L$ was measured using $R^n(v)$ with $N = 0$, with which value the denominator is an excellent measure of the size of the phenomenon being modelled. By definition $R^0(v) = 0$. Also, if this wave were fully reflected at $x = L$ then subsequently $R^n(v)$ would equal 1. Equally, $R^n(v)$ would subsequently equal zero if the wave exited without reflection. In fact, $R^n(v)$ remained at zero until the front edge of the wave struck the boundary and slowly rose to a final value of 1% after the wave exited. Subsequent to that $R^n(v)$ was constant until the bulk of the reflected wave was transmitted through the boundary at $x = 0$, which caused $R^n(v)$ to fall further to a value of 0.1%. The same test was done for each of the other $\{m\}_{pv}$-waves, using initial states as described by eq. (4.44). For each integration $R^n(v)$ subsequent to the exit of the shape was approximately the same size, the largest value being $R^n(v) = 1.3\%$ for the $\{10\}_{pv}$-wave.

Test 2. Are the boundaries transparent for incoming potential vorticity waves?

The purpose of this experiment is to show that potential vorticity waves from an external source can be injected accurately into the integration area. Thus it is assumed that a $\{5\}_{pv}$ wave, initially centered outside the area at $x = -2L/5$, crosses the boundary at $x = 0$ during the integration, moving at a velocity $u_0 = 25$ ms^{-1}. Can the boundary conditions derived in section 4.2 accurately model this scenario?

To generate the boundary fields a forecast was run on the host area with the initial state described by eq. (4.44) with x replaced with x^h and $L/2$ replaced with $L^h/2 - L/2 - 2L/5$. This was integrated for 9 h, at which time the $\{5\}_{pv}$ wave was centered at $x^h = L^h/2 - 90$ km, 410 km inside the guest integration area. The fields $\boldsymbol{\rho}^h$, $\mathbf{u}^h, \mathbf{v}^h$ and $p^h_{\frac{1}{2}}$ at $x^h = L^h/2 - L/2 + \Delta x/2$ were computed at every time step and written to a file. During the guest forecast these fields were read in at each time step and used to compute the boundary fields for each mode, m, using eq. (2.33).

$R^n(v)$ with N chosen as the last step in the forecast was used to measure the

transparency of the boundary at $x = 0$. At time step N the bulk of the shape was inside the integration area, see Fig. 7, making the denominator in eq. (4.43) a good measure of the size of the phenomenon being measured. $R^0(v) = 0$ by definition, and $R^n(v) = 0$ for an external wave that enters perfectly; also, $R^n(v) = 1$ for a wave that fails totally to be transmitted through the inflow boundary.

The similarity of Fig. 7 to Fig. 6 is an indication that the wave has been transmitted accurately through the boundary, a fact confirmed by the value of $R^N(v) = 0.04\%$.

Test 3. Are the boundaries still transparent for outgoing gravity waves?

The basis for deriving semi-transparent boundary conditions is the assumption that f/s can be regarded as a small parameter. From eqs. (2.15) and (2.17) it is clear that this assumption is tested most severely for waves such that $u_0/c_m \gg 1$. Therefore the question addressed by this test is: how transparent is the boundary at $x = L$ to an outgoing $\{10\}_+$-wave, for which $u_0/c_{10} = 15.6$ when $u_0 = 25$ ms^{-1} ? The initial state, situated at $L/2$ is

$$\begin{aligned} p_j(x,0) &= E_{j,m}[\breve{Q}_m]^{(0)}_{1,1}\frac{\partial b_1}{\partial t}\Big(x, \frac{L}{2}, 0, \frac{L}{10}\Big), \\ u_j(x,0) &= E_{j,m}[\breve{Q}_m]^{(0)}_{2,1}\frac{\partial b_1}{\partial t}\Big(x, \frac{L}{2}, 0, \frac{L}{10}\Big), \\ v_j(x,0) &= E_{j,m}[\breve{Q}_m]^{(1)}_{3,1} f b_1\Big(x, \frac{L}{2}, 0, \frac{L}{10}\Big), \end{aligned} \tag{4.45}$$

with $m = 10$; see Fig. 8. The fields are normalized such that the maximum $u'(x,0)$ is 10 ms^{-1}. On starting the integration this wave moves in the $+x$-direction with a velocity of approximately 26.6 ms^{-1}.

In order to make this test meaningful the host model fields were used *solely* to measure the rms errors. Thus, in using eq. (2.28) the $\hat{\mathbf{W}}$ were chosen as follows for each mode $m = 1, 5$: at $x = 0$, $\hat{\mathbf{W}} = (0, 0, \hat{W}^g_3)^T$ and at $x = L$, $\hat{\mathbf{W}} = (\hat{W}^g_1, \hat{W}^g_2, 0)^T$; and as follows for each mode $m = 6, 10$: at $x = 0$, $\hat{\mathbf{W}} = (0, 0, 0)^T$ and at $x = L$, $\hat{\mathbf{W}} = (\hat{W}^g_1, \hat{W}^g_2, \hat{W}^g_3)^T$.

The error caused by any reflection at $x = L$ was measured using $R^n(u)$ with $N = 0$, at which time the denominator is an excellent measure of the size of the phenomenon being modelled. By definition $R^0(u) = 0$. Also, if this wave were fully reflected at $x = L$

then subsequently $R^n(u)$ would equal 1. Equally, $R^n(u)$ would subsequently equal zero if the wave exited without reflection. In fact, $R^n(u)$ remained at zero until the front edge of the wave struck the boundary and slowly rose to a final value of 2.2% as the wave exited. Subsequent to that $R^n(u)$ oscillated between 1.3% and 2.2%. The integration is stable but the presence of the dispersion does reduce the transparency of the boundary a little.

5. Conclusion

The objective of this paper was to demonstrate that the approach to open boundaries advocated by Engquist and Majda (1977) is sufficiently robust to accommodate potential vorticity waves when baroclinic waves are also present. For the two-layer model a transparency of the boundaries of better than 97.5% was demonstrated. For the multi-level model the results were also encouraging. For outgoing potential vorticity waves a transparency of better than 98.7% was demonstrated, and for incoming potential vorticity waves a transparency of 99.9% was demonstrated. Equally important, the boundaries were shown to be stable and 97.8% transparent for the potentially most troublesome slowest gravity inertia waves.

In section 2 it was shown that the derived boundary conditions caused the fields to drift to unphysical values if the boundary fields at time zero did not agree with the initial fields on the boundary. By implication, if at any time during the integration a jump discontinuity is introduced at the boundary the fields can be expected to drift to unphysical values during the remainder of the integration. Therefore for these boundary conditions to work in a more realistic nested setting, in which the host model time and space discretizations differ from those of the guest model, it is essential that the space and time interpolation of the fields from the host grid to the guest grid produce well-behaved fields. (McDonald, 2003, gives a practical demonstration of a forecast being improved by increasing the smoothness of the boundary fields).

Acknowledgment. Thanks to Jim Hamilton for help with the graphics. Thanks to the HIRLAM group for their support and encouragement.

APPENDIX A

In this appendix the matrices appropriate to section 3 are tabulated. From eqs. (3.1)-(3.6) the matrices $\mathbf{A}$ and $\mathbf{B}$ are

$$\mathbf{A} = \begin{bmatrix} \bar{u} & 0 & H_1 & H_2 & 0 & 0 \\ 0 & \bar{u} & 0 & H_2 & 0 & 0 \\ g & 0 & \bar{u} & 0 & 0 & 0 \\ g'' & g' & 0 & \bar{u} & 0 & 0 \\ 0 & 0 & 0 & 0 & \bar{u} & 0 \\ 0 & 0 & 0 & 0 & 0 & \bar{u} \end{bmatrix}, \tag{A1}$$

and

$$\mathbf{B} = \begin{bmatrix} 1 & 0 & 0 & 0 & 0 & 0 \\ 0 & 1 & 0 & 0 & 0 & 0 \\ 0 & 0 & 1 & 0 & -f/s & 0 \\ 0 & 0 & 0 & 1 & 0 & -f/s \\ 0 & 0 & f/s & 0 & 1 & 0 \\ 0 & 0 & 0 & f/s & 0 & 1 \end{bmatrix}. \tag{A2}$$

From these, $\mathbf{A}^{-1}$ and $\mathbf{A}^{-1}\mathbf{B}$ follow:

$$\mathbf{A}^{-1} = \bar{u}^2 D_A^{-1} \begin{bmatrix} \bar{u}G_2' & \bar{u}g'H_2 & -H_1G_2' & -\bar{u}^2H_2 & 0 & 0 \\ H_2\bar{u}g'' & \bar{u}G_{12} & -H_2g''H_1 & -H_2G_1 & 0 & 0 \\ -gG_2' & -gg'H_2 & \bar{u}G_2 & g\bar{u}H_2 & 0 & 0 \\ -\bar{u}^2g'' & -g'G_1 & \bar{u}g''H_1 & \bar{u}G_1 & 0 & 0 \\ 0 & 0 & 0 & 0 & \frac{D_A}{\bar{u}^3} & 0 \\ 0 & 0 & 0 & 0 & & \frac{D_A}{\bar{u}^3} \end{bmatrix}, \tag{A3}$$

where the determinant of $\mathbf{A}$ is

$$D_A = \bar{u}^2[\bar{u}^4 - \bar{u}^2 g(H_1 + H_2) + gg'H_1H_2], \tag{A4}$$

and

$$G_1 = (\bar{u}^2 - gH_1); \quad G_2 = (\bar{u}^2 - gH_2); \quad G_2' = (\bar{u}^2 - g'H_2); \quad G_{12} = G_1 + G_2 - G_2'. \tag{A5}$$

Finally,

$$\mathbf{A}^{-1}\mathbf{B} = \bar{u}^2 D_A^{-1} \begin{bmatrix} \bar{u}G_2' & \bar{u}g'H_2 & -H_1G_2' & -\bar{u}^2H_2 & \frac{f}{s}H_1G_2' & \frac{f}{s}\bar{u}^2H_2 \\ H_2\bar{u}g'' & \bar{u}G_{12} & -H_2g''H_1 & -H_2G_1 & \frac{f}{s}H_2g''H_1 & \frac{f}{s}H_2G_1 \\ -gG_2' & -gg'H_2 & \bar{u}G_2 & g\bar{u}H_2 & -\frac{f}{s}\bar{u}G_2 & -\frac{f}{s}g\bar{u}H_2 \\ -\bar{u}^2g'' & -g'G_1 & \bar{u}g''H_1 & \bar{u}G_1 & -\frac{f}{s}\bar{u}g''H_1 & -\frac{f}{s}\bar{u}G_1 \\ 0 & 0 & \frac{f}{s}\frac{D_A}{\bar{u}^3} & 0 & \frac{D_A}{\bar{u}^3} & 0 \\ 0 & 0 & 0 & \frac{f}{s}\frac{D_A}{\bar{u}^3} & 0 & \frac{D_A}{\bar{u}^3} \end{bmatrix}. \quad (A6)$$

Using the following definitions,

$$c_0 = \left\{\frac{g}{2}(H_1+H_2)\left[1+\left(1-\frac{4g'H_1H_2}{g(H_1+H_2)^2}\right)^{1/2}\right]\right\}^{1/2}, \quad (A7)$$

$$c_1 = \left\{\frac{g}{2}(H_1+H_2)\left[1-\left(1-\frac{4g'H_1H_2}{g(H_1+H_2)^2}\right)^{1/2}\right]\right\}^{1/2}; \quad (A8)$$

$$Y_0 = \left\{1+\frac{f^2}{s^2}\left(1-\frac{\bar{u}^2}{c_0^2}\right)\right\}^{\frac{1}{2}}; \qquad Y_1 = \left\{1+\frac{f^2}{s^2}\left(1-\frac{\bar{u}^2}{c_1^2}\right)\right\}^{\frac{1}{2}}, \quad (A9)$$

the six eigenvalues of $\mathbf{A}^{-1}\mathbf{B}$ are

$$\lambda_1 = \frac{1}{\bar{u}+c_0} + \frac{c_0(1-Y_0)}{\bar{u}^2-c_0^2}; \qquad \lambda_2 = \frac{1}{\bar{u}+c_1} + \frac{c_1(1-Y_1)}{\bar{u}^2-c_1^2}; \qquad \lambda_3 = \frac{1}{\bar{u}};$$

$$\lambda_4 = \frac{1}{\bar{u}}; \qquad \lambda_5 = \frac{1}{\bar{u}-c_1} - \frac{c_1(1-Y_1)}{\bar{u}^2-c_1^2}; \qquad \lambda_6 = \frac{1}{\bar{u}-c_0} - \frac{c_0(1-Y_0)}{\bar{u}^2-c_0^2}, \quad (A10)$$

corresponding to four gravity-inertia waves and two potential vorticity waves. The left eigenvectors associated with these eigenvalues are, respectively

$$\mathbf{l}_1 = n_1(s)\left(a_1, -1, \frac{H_1a_1Y_0}{c_0}, -\frac{c_0Y_0}{g'}, \frac{f}{s}\frac{\bar{u}H_1a_1}{c_0^2}, -\frac{f}{s}\frac{\bar{u}}{g'}\right),$$

$$\mathbf{l}_2 = n_2(s)\left(a_0, -1, \frac{H_1a_0Y_1}{c_1}, -\frac{c_1Y_1}{g'}, \frac{f}{s}\frac{\bar{u}H_1a_0}{c_1^2}, -\frac{f}{s}\frac{\bar{u}}{g'}\right),$$

$$\mathbf{l}_3 = n_3(s)\left(\frac{f}{s}\frac{\bar{u}}{H_1}, -\frac{f}{s}\frac{\bar{u}}{H_1}, \frac{f}{s}, 0, 1, 0\right),$$

$$\mathbf{l}_4 = n_4(s)\left(0, \frac{f}{s}\frac{\bar{u}}{H_2}, 0, \frac{f}{s}, 0, 1\right),$$

$$\mathbf{l}_5 = n_5(s)\left(a_0, -1, -\frac{H_1a_0Y_1}{c_1}, \frac{c_1Y_1}{g'}, \frac{f}{s}\frac{\bar{u}H_1a_0}{c_1^2}, -\frac{f}{s}\frac{\bar{u}}{g'}\right),$$

$$\mathbf{l}_6 = n_6(s)\left(a_1, -1, -\frac{H_1a_1Y_0}{c_0}, \frac{c_0Y_0}{g'}, \frac{f}{s}\frac{\bar{u}H_1a_1}{c_0^2}, -\frac{f}{s}\frac{\bar{u}}{g'}\right),$$

$$(A11)$$

where $n_i(s)$ are arbitrary normalization factors, and $a_i = 1 - gH_1/c_i^2$.

(The computer algebra system 'maxima' was used to compute the following: $\mathbf{A}^{-1}$, D_A, $\mathbf{A}^{-1}\mathbf{B}$, and the determinant of $\mathbf{A}^{-1}\mathbf{B} - \lambda\mathbf{I}$. Setting the latter determinant to zero furnishes the eigenvalues. Once these are known the left eigenvectors can be calculated.)

The matrix $\mathbf{Q}^{-1}$ is chosen such that $n_i = 1$ giving, from eq. (A11)

$$[\mathbf{Q}^{-1}]^{(0)} = \begin{bmatrix} a_1 & -1 & \frac{H_1 a_1}{c_0} & -\frac{c_0}{g'} & 0 & 0 \\ a_0 & -1 & \frac{H_1 a_0}{c_1} & -\frac{c_1}{g'} & 0 & 0 \\ 0 & 0 & 0 & 0 & 1 & 0 \\ 0 & 0 & 0 & 0 & 0 & 1 \\ a_0 & -1 & -\frac{H_1 a_0}{c_1} & \frac{c_1}{g'} & 0 & 0 \\ a_1 & -1 & -\frac{H_1 a_1}{c_0} & \frac{c_0}{g'} & 0 & 0 \end{bmatrix}, \qquad (A12)$$

$$[\mathbf{Q}^{-1}]^{(1)} = \begin{bmatrix} 0 & 0 & 0 & 0 & \frac{\bar{u} H_1 a_1}{c_0^2} & -\frac{\bar{u}}{g'} \\ 0 & 0 & 0 & 0 & \frac{\bar{u} H_1 a_0}{c_1^2} & -\frac{\bar{u}}{g'} \\ \frac{\bar{u}}{H_1} & -\frac{\bar{u}}{H_1} & 1 & 0 & 0 & 0 \\ 0 & \frac{\bar{u}}{H_2} & 0 & 1 & 0 & 0 \\ 0 & 0 & 0 & 0 & \frac{\bar{u} H_1 a_0}{c_1^2} & -\frac{\bar{u}}{g'} \\ 0 & 0 & 0 & 0 & \frac{\bar{u} H_1 a_1}{c_0^2} & -\frac{\bar{u}}{g'} \end{bmatrix}, \qquad (A13)$$

$$\mathbf{Q}^{(0)} = \frac{1}{N_Q^0} \begin{bmatrix} 1 & -1 & 0 & 0 & -1 & 1 \\ a_0 & -a_1 & 0 & 0 & -a_1 & a_0 \\ \frac{g}{c_0} & -\frac{g}{c_1} & 0 & 0 & \frac{g}{c_1} & -\frac{g}{c_0} \\ \frac{a_0 c_0}{H_2} & -\frac{a_1 c_1}{H_2} & 0 & 0 & \frac{a_1 c_1}{H_2} & -\frac{a_0 c_0}{H_2} \\ 0 & 0 & N_Q^0 & 0 & 0 & 0 \\ 0 & 0 & 0 & N_Q^0 & 0 & 0 \end{bmatrix}, \qquad (A14)$$

$$\mathbf{Q}^{(1)} = \frac{1}{N_Q^0} \begin{bmatrix} 0 & 0 & -\frac{\bar{u} N_Q^0}{g} & 0 & 0 & 0 \\ 0 & 0 & -\frac{\bar{u} N_Q^0 a_0 a_1}{g} & -\frac{\bar{u} N_Q^0}{g'} & 0 & 0 \\ 0 & 0 & 0 & 0 & 0 & 0 \\ 0 & 0 & 0 & 0 & 0 & 0 \\ -\frac{g(\bar{u}+c_0)}{c_0^2} & \frac{g(\bar{u}+c_1)}{c_1^2} & 0 & 0 & \frac{g(\bar{u}-c_1)}{c_1^2} & -\frac{g(\bar{u}-c_0)}{c_0^2} \\ -\frac{a_0(\bar{u}+c_0)}{H_2} & \frac{a_1(\bar{u}+c_1)}{H_2} & 0 & 0 & \frac{a_1(\bar{u}-c_1)}{H_2} & -\frac{a_0(\bar{u}-c_0)}{H_2} \end{bmatrix}, \qquad (A15)$$

where

$$N_Q^0 = \frac{2gH_1(c_1^2 - c_0^2)}{c_1^2 c_0^2}. \qquad (A16)$$

REFERENCES

Daley R., 1979: An application of non-linear normal mode initialization to an operational forecast model. *Atmos. Ocean* **17** 97-124 .

Doetsch, G., 1971: *Guide to the Application of the Laplace and Z-Transforms* Van Nostrand Reingold Co., 240pp.

Engquist, B., and A. Majda, 1977: Absorbing boundary conditions for the numerical simulation of waves. *Math. Comput.,* **31**, 629-651.

Gill, A.E., 1982: *Atmosphere-Ocean Dynamics.* Orlando: Academic Press, 662pp.

Hagstrom, T., 1999: Radiation boundary conditions for the numerical simulation of waves. *Acta Numerica*, 47-106.

Ince, E.L., 1956: *Ordinary Differential Equations.* Dover Publications Inc. 558pp.

Kalnay, E., 2003: *Atmospheric Modeling, Data Assimilation, and Predictability* . Cambridge University Press. 341pp.

McDonald, A., 2002: A step toward transparent boundary conditions for meteorological models. *Mon. Wea. Rev.,* **130**, 140-151.

McDonald, A., 2003: Transparent boundary conditions for the shallow water equations: testing in a nested environment. *Mon. Wea. Rev.* **131**, 698-705.

McDonald, A., 2005: Transparent lateral boundary conditions for baroclinic waves: a study of two elementary systems of equations. *Tellus* **57A** 171-182.

Robert, A.J., 1966: The integration of a low order spectral form of the primitive meteorological equations. *J. Meteor. Soc. Japan, Ser. 2,* **44**, 237-245.

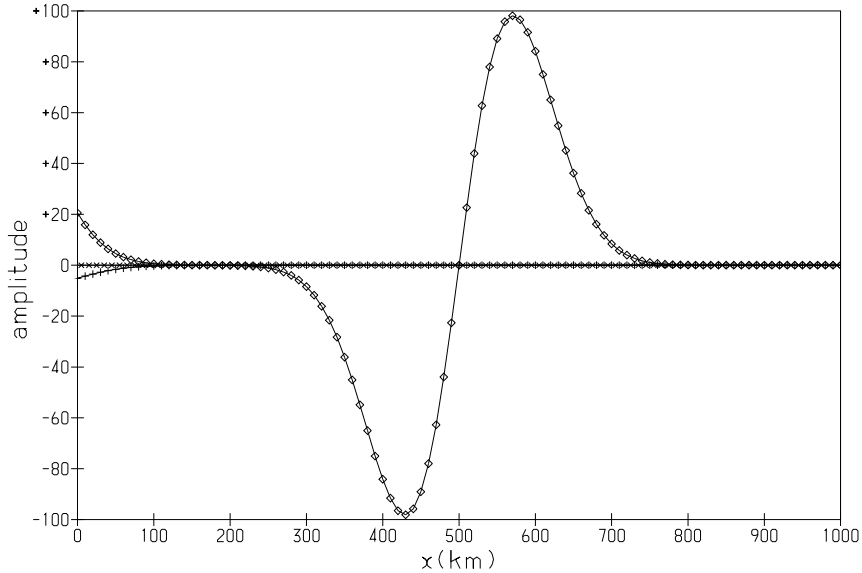

Figure 1: *The fields $g\eta, \bar{c}u$ and v at time step zero. The field $g\eta$, whose amplitude is given in m^2s^{-2} is represented by diamonds; the amplitude of $\bar{c}u$ (m^2s^{-2} also) is represented by 'exes'; the amplitude of v (ms^{-1}) is represented by 'plusses'.*

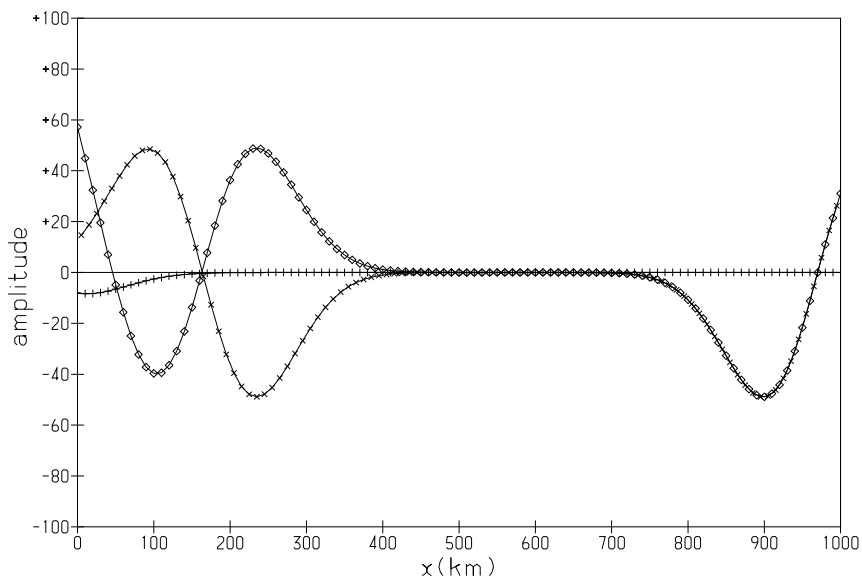

Figure 2: *Same as Fig. 1, but after 22.5 mins. of integration.*

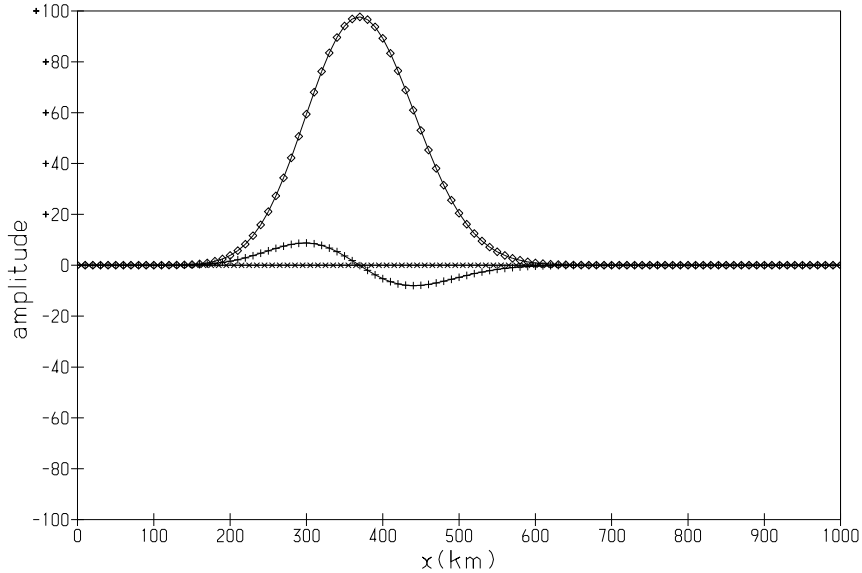

Figure 3: *Same as Fig. 1, but after 167 mins. of integration.*

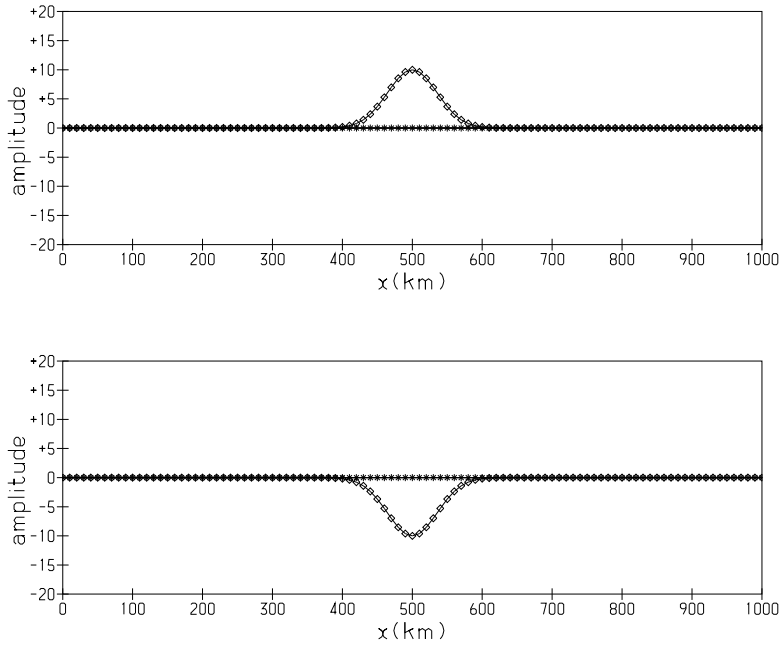

Figure 4: *The fields* η_1, u_1 *and* v_1 *(top picture) and* η_2, u_2 *and* v_2 *(bottom picture) at time zero. The* η*-amplitudes are in metres and are displayed as diamonds. The* u*- and* v*-amplitudes are in* ms^{-1} *and the former are displayed as 'exes', and the latter as 'plusses'.*

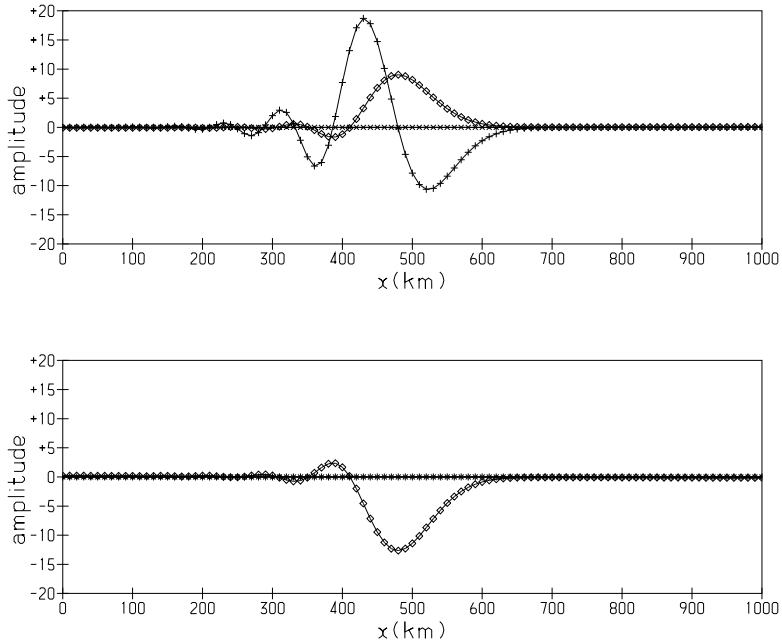

Figure 5: *Same as Fig. 4 except that these are the fields after 250 mins. of integration.*

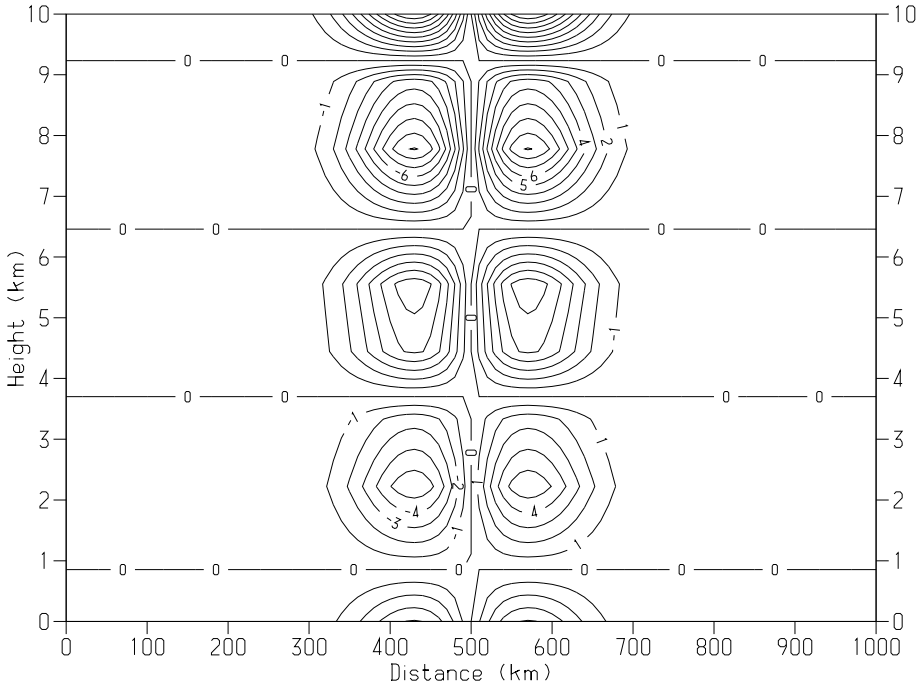

Figure 6: *The wind anomaly v' for the $\{5\}_{pv}$-wave at the initial time.*

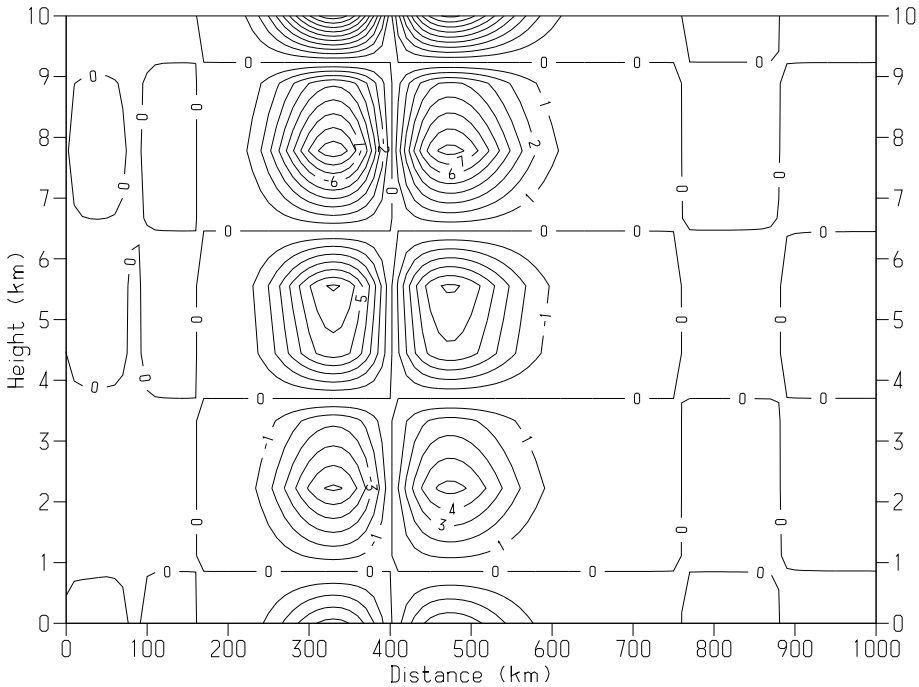

Figure 7: *The wind anomaly v' for the injected $\{5\}_{pv}$-wave after 9 h of integration.*

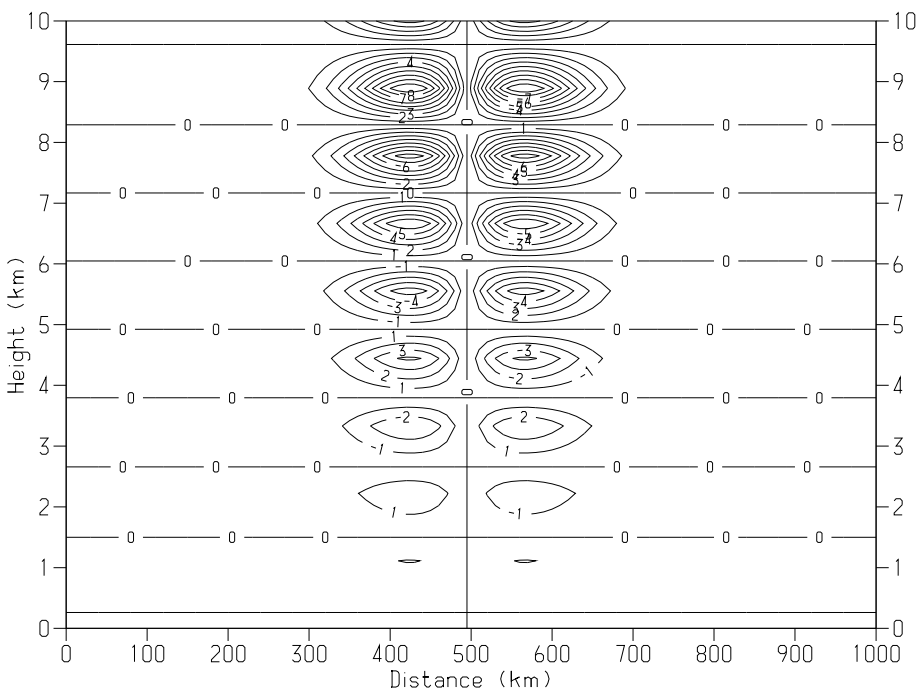

Figure 8: *The wind anomaly u' for the $\{10\}_{+}$-wave at the initial time.*